Converted-wave seismic exploration: applications

Robert R. Stewart, James E. Gaiser, R. James Brown, and Don C. Lawton

ABSTRACT

Converted seismic waves (P-to-S on reflection) are being increasingly used to explore for subsurface targets. Rapid advancements in multicomponent acquisition methods and processing techniques have led to numerous applications for P-S images. Uses that have arisen include sand/shale differentiation, carbonate identification, definition of interfaces with low P-wave contrast, anisotropy analysis, imaging through gas zones, shallow high-resolution imaging, and reservoir monitoring. Marine converted-wave analysis using 4-C recordings (a three-component geophone plus a hydrophone) has generated some remarkable images.

BACKGROUND

A great richness of wavetypes propagate in an exploration seismic survey; hopefully, they encounter a significant richness of resources. The converted-wave (P-S) method of seismic exploration uses P energy propagating downward and reflecting back upward as an S-wave from its deepest point of penetration. The goal of this imaging is to obtain a measure of subsurface S-wave properties relating to rock type and saturation - usually in addition to the P-wave values. We want the additional S-wave properties because a P-wave image, and even a set of P-wave derived rock properties, is often not enough to fully characterize the subsurface and its fluids. P-S surveys are a relatively inexpensive, broadly applicable, and effective way to obtain S-wave information. If we do have P-S reflectivity, what can it be used for? Various authors (e.g., Kristiansen, 2000) have suggested or shown a number of applications of P-S data that include:

- Providing another section with independent properties (e.g., velocity, multiples, tuning);

- Imaging interfaces with low *P*-wave contrast but significant *S*-wave change;

- More detailed shallow imaging; enhanced fault imaging

- Imaging through gas chimneys, shale diapirs, mud volcanoes and beneath salt and basalt;

- *P-P* interpretive constraint via V_p/V_s analysis and correlation;

- Calibrating *P*-wave bright spots;

- Augmenting conventional AVO analysis for density and velocity;

- Investigating anisotropy for processing as well as fracture density and orientation;

- Using V_p/V_s for lithology discrimination (e.g., sand/shale);

- Monitoring reservoir changes (time-lapse or 4-D).

Let's look in more detail at some of these applications.

CASE HISTORIES

Lithology detection

P-wave imaging has proven particularly adept at making structural pictures of the subsurface, that is, providing an image of strata interfaces in reflection time. However, beyond the configuration of interfaces, we would like to know what kind of rock and fluids are in the section. P-wave images are often limited or ambiguous in these regards. S-wave measurements provide additional constraint on the rock properties (especially on density and rigidity contrasts). Much P-S analysis is targeted at finding an S-wave velocity or determining a Vp/Vs value. Both Vs and Vp/Vs can be good indicators of rock type, especially in combination with Vp. Garotta et al. (1985) show *P-S* and *P-P* data for a Viking sand channel reservoir in the Winfield oil field, Alberta. They find amplitude anomalies on the *P-S* data correlating with the known boundaries of the reservoir. They also used isochron ratios to determine V_p/V_s and Poisson's ratios. They interpret low Poisson's ratios as differentiating sand from the neighbouring shales.

Nazar and Lawton (1993) used AVO stacks, *P-P*, and *P-S* sections to analyse the productive regions of the Carrot Creek field (Figure 1).
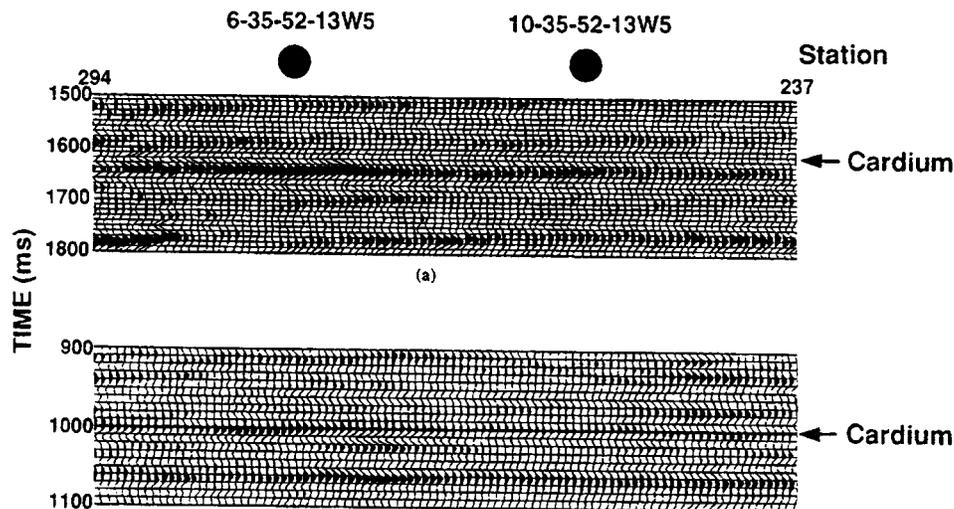
Figure 1. Detail of the *P-S* (top) and *P-P* (bottom) sections from Carrot creek, Alberta. Note the amplitude anomaly on the *P-S* section at the Cardium conglomerate level (from Nazar and Lawton, 1993).

The oil-saturated conglomerate in this region is not well imaged by conventional data but is apparent on *P-S* sections as a brightening in amplitude. This relative

brightening is partially due to differences in tuning between *P-P* and *P-S* reflections and the relatively high S-wave velocity of the Cardium conglomerate.

Miller et al. (1998) found significant variations in V_p/V_s (from P-P and P-S isochron ratios) in a carbonate play in Lousana, Alberta. The V_p/V_s values in the Cretaceous section (ranging from 2.2-2.5) are indicative of a clastic section while those in the Paleozoic (1.5-2.0) are characteristic of carbonate rocks. The lower values in the Paleozoic, from shot point 172 to 212, are coincident with an underlying oil-bearing reef. They interpret this anomaly as being associated with dolomitization.

A series of seismic experiments in the Blackfoot region of Alberta were conducted to identify sand reservoir facies from non-reservoir rocks (Stewart et al., 1996). The surveys included broad-band 3C-2D data, full 3C-3D data, and 2-D and 3-D VSP surveys. The processed broad-band 2-D lines tie reasonably well. Using this tie and picking isochrons, we can calculate an interval V_p/V_s value. We take an interval that includes the productive channel sand. There is a reasonable correlation of V_p/V_s anomalies and known oil production. The field was originally discovered and developed using *P*-wave amplitude anomalies (Figure 2); however, there are also false positives (amplitude anomalies) not associated with sand channels. *P-P* isochrons are also indicative of the channel but again with some ambiguity. The *P-S* amplitude seems to give a more definitive (but lower resolution) image of the sand channel (Figure 2). A *P-S* isochron including the channel is perhaps more compelling (Figure 3). The V_p/V_s maps, calculated from *P-P* and *P-S* isochron ratios, are another strong indicator of the reservoir sand channel trend (Figure 3). A further Blackfoot 3C-3D survey (Goodway and Tessman, 2000) was conducted in 1999 with the I/O Vectorseis[TM] digital 3-C geophone. This survey produced similar results to the previous 1995 3C-3D survey. This independent test provided evidence as to the repeatability of results and will be useful for time-lapse analysis.
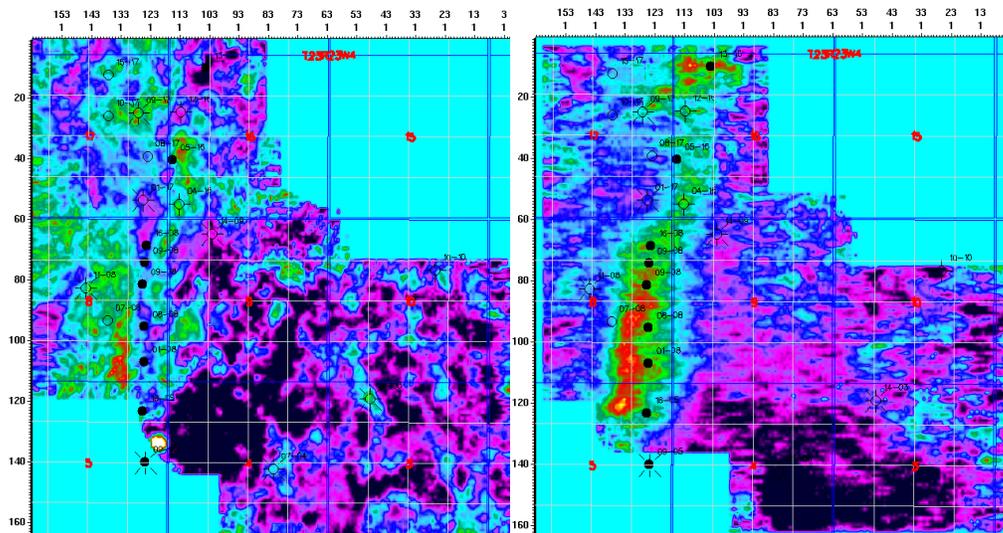
Figure 2. P-P (left) and P-S (right) time slices at the interpreted sand channel level from the Blackfoot 3C-3D survey.
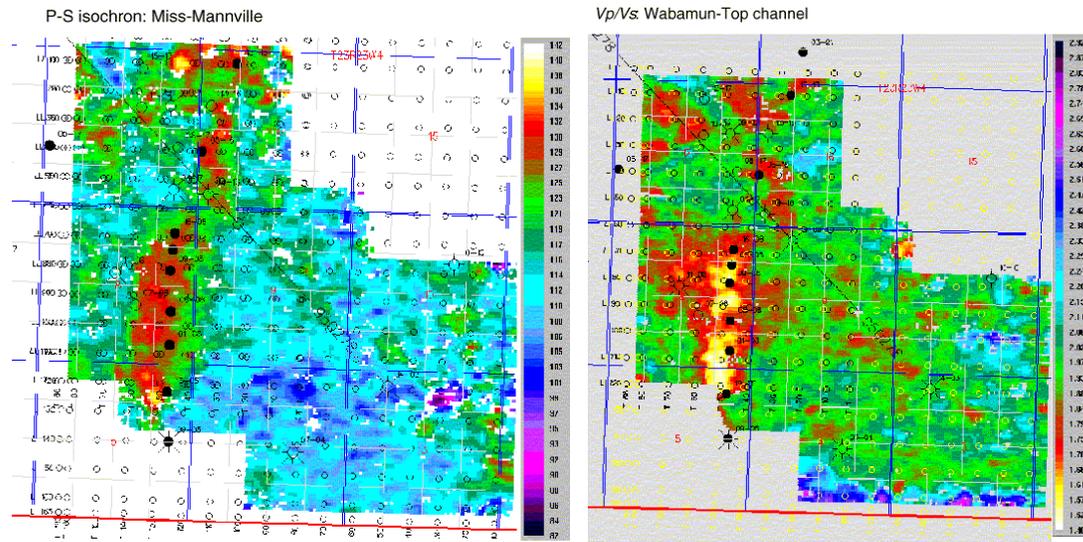
Figure 3. P-S isochron (left) between the Mannville and Mississippian horizons and the Vp/Vs value as determined from the P-P and P-S isochrons between the interpreted top of the channel and Wabamun horizons.
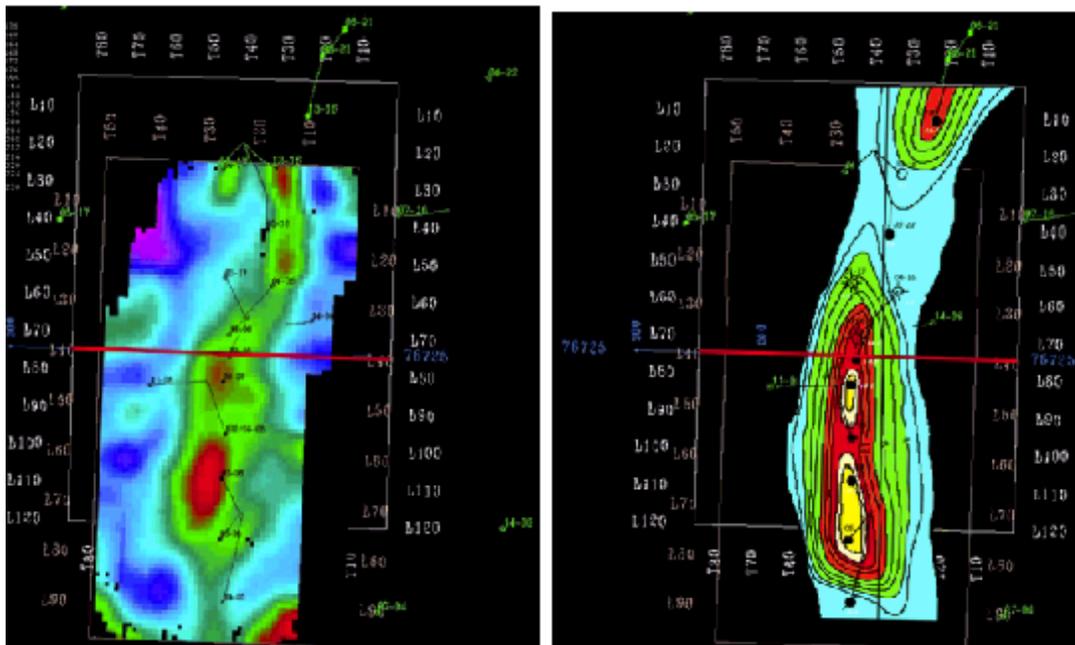
Figure 4. A second 3C-3D survey in 1999 conducted with VectorSeis[TM] digital geophones (Goodway and Tessman, 2000) gave another fairly consistent Vp/Vs anomaly (left) that correlates with net sand thickness (right).

MacLeod et al. (1999a) show a case of converted waves successfully delineating sand channels incased in shale at the Alba field in the North Sea. A strong contrast in *S*-wave velocity is associated with the sand reservoir. Although *P*-wave velocity is sensitive to changes in fluid at the OWC, there is a relatively small contrast in *P*-wave velocity due to the change in lithology (Figure 5). A 4-C OBC survey was conducted

over Alba field to delineate the reservoir extent. Figure 6 illustrates the dramatically improved imaging of reservoir sands by *P-S* data relative to streamer *P*-wave data for a 2-D section.
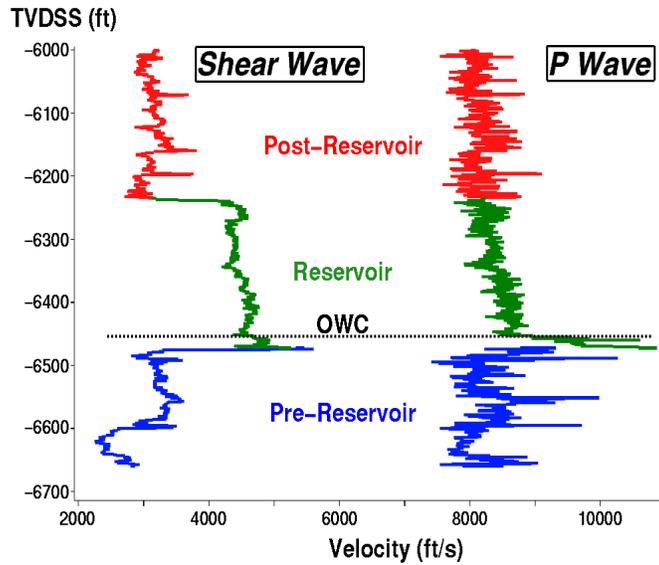
Figure 5. The dipole sonic log through the Alba reservoir sand shows a large contrast in shear wave velocity and a small contrast in *P*-wave velocity with the surrounding shales (after MacLeod et al., 1999b).
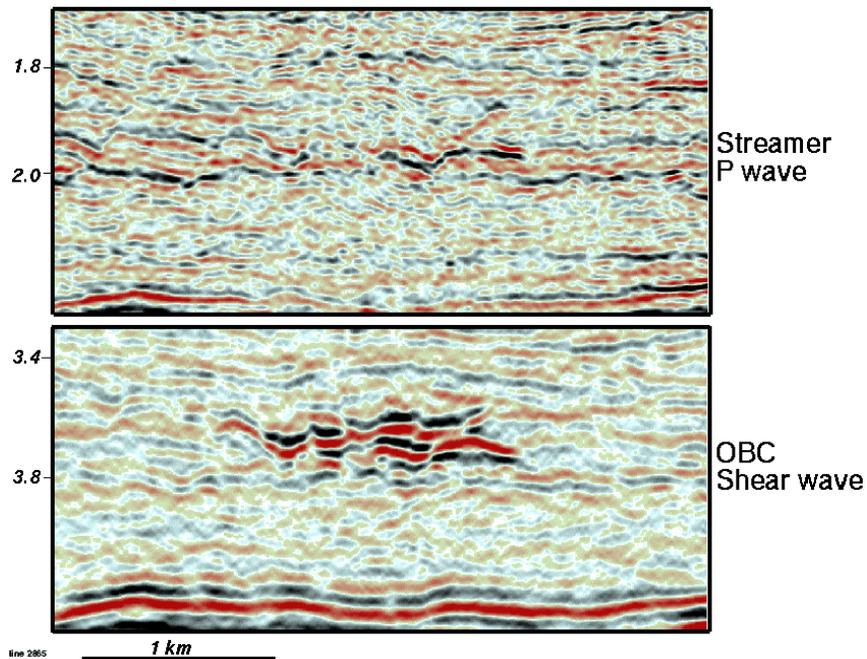
Figure 6. Converted-wave image from the "15 Area" showing dramatically improved imaging relative to the streamer *P*-wave data. The outline of the Alba field is clearly seen only in the converted-wave data (after MacLeod et al., 1999b).

The impact of the 4-C OBC survey on the development of Alba has been positive (MacLeod, et al., 1999b). To date, several successful wells have been drilled based primarily on the interpretation of the new converted-wave data. There are excellent ties between lithologies encountered in these wells and pseudo-elastic impedance computed from the converted-wave seismic response. Also, the *P-S* data have provided new insights into the complex geometry of the Alba field, suggesting significant post-depositional deformation of the turbidite channel.

Valenciano et al. (2000) discuss a 3C-3D survey conducted over the Zuata oil field in eastern Venezuela. They report that there is little acoustic impedance difference between the overlying shales and sand reservoir rocks. However, the S-wave velocity varies significantly from shale to sand (Figure 7). They use these rock properties, seismic inversion, and neural net classification to indicate lithology type (Figure 8).
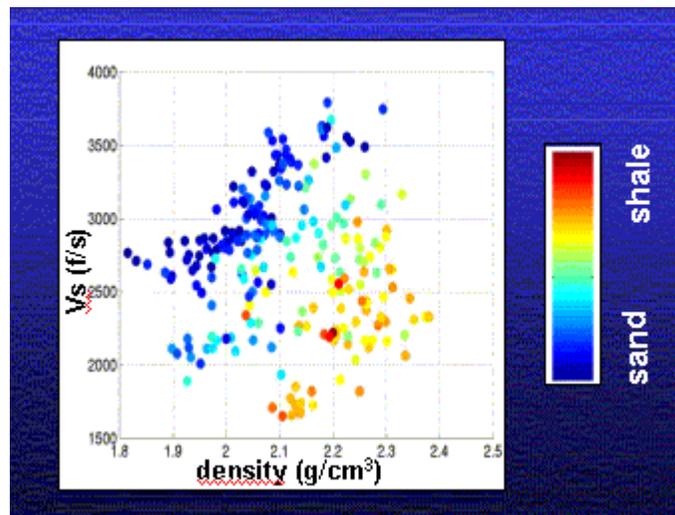
Figure 7. S-wave velocity versus density from well logs in the Zuata heavy oil field, Venezuela. The S velocity of the sands is considerably higher than that of the shales.
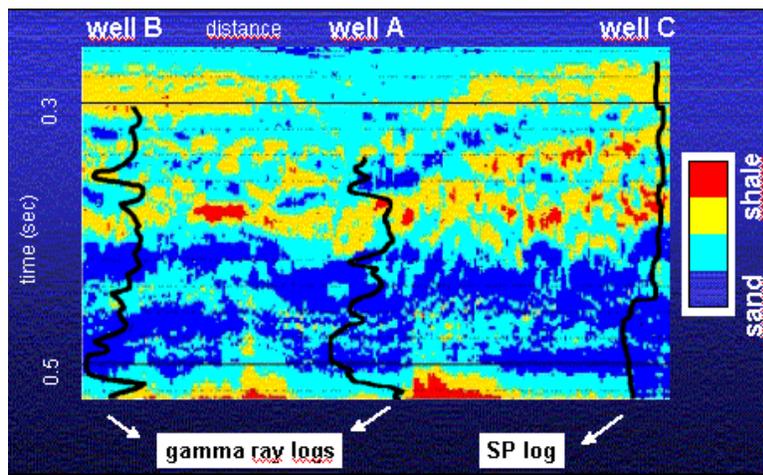
Figure 8. Section from the Zuata heavy oil field, Venezuela. The S-wave inversions have been converted to sand/shale estimates via a neural net process. SP and gamma ray logs are overlain for comparison.

Van Dok and Gaiser (2000) describe three 3-C surveys over the Morrow formation in the southern United States. The Eva South 3C-3D survey, in the panhandle of Oklahoma, shows anomalous P-S amplitudes that correlate with net pay thickness (Figure 9).
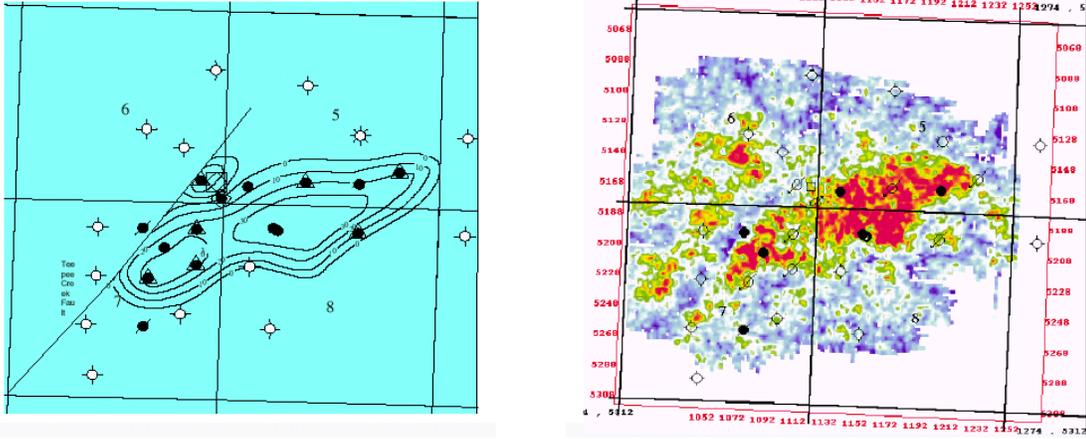
Figure 9. The Eva South 3C-3D survey shows net pay thicknesses (left) and the reasonably well correlating P-S amplitudes (right) at the reservoir level.

They also used an automatic event correlation technique on multicomponent data from the Cave West survey in southwestern Kansas. P-P and P-S sections drawn from the 3-D volumes are shown in Figure 10. They found that Vp/Vs values from the automatic technique correlated reasonably with sand thickness values from the wells (Figure 11). There is an interesting indication (by high Vp/Vs values) of a shale zone in the NW corner of the survey which is confirmed by well results.
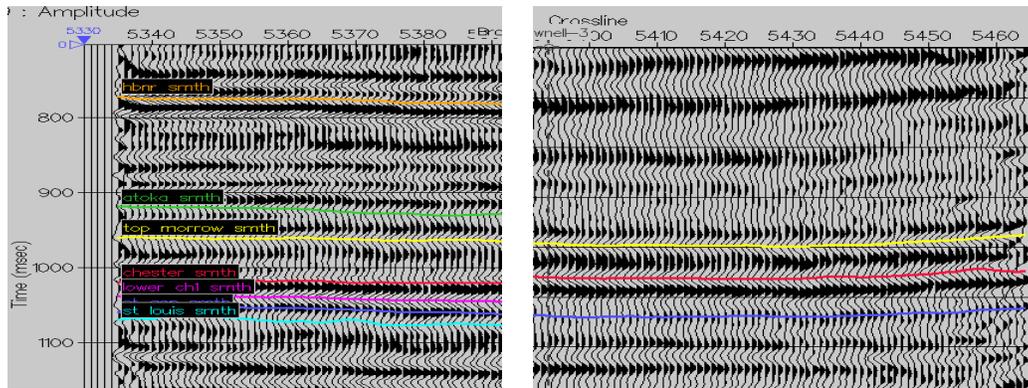
Figure 10. P-P (left) and P-S (right) sections from the Cave West, Oklahoma 3C-3D survey. The top of the Morrow sand is highlighted in yellow.
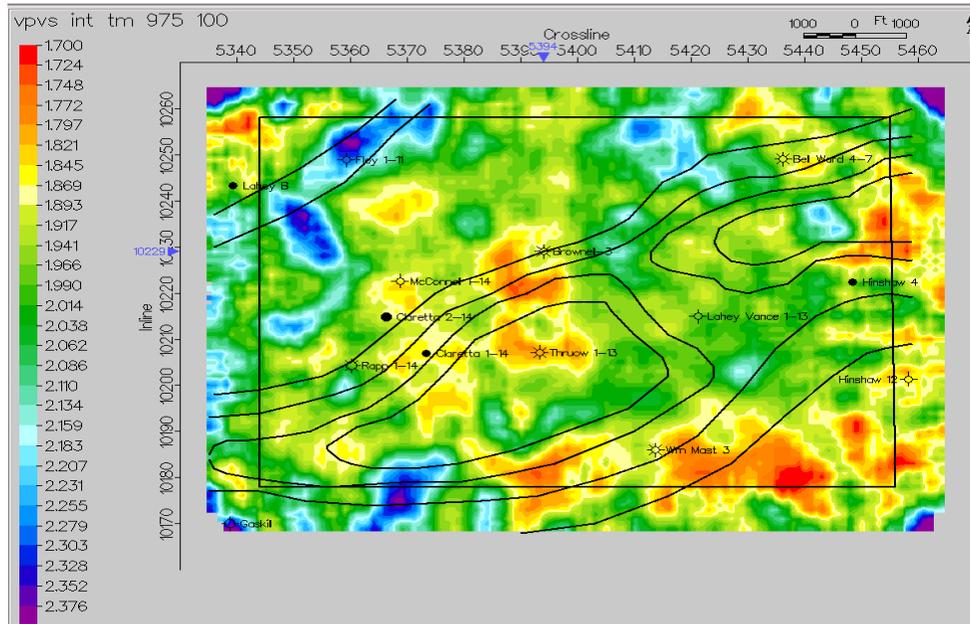
Figure 11. Map of the automatically determined Vp/Vs value over the Cave West, Oklahoma survey. The interval of Vp/Vs analysis over the Morrow formation. Note the high values in the northwest corner that are interpreted to indicate high shale content (which is confirmed by well results).

Further down in the section, the St. Gen formation is encountered. A coherencey plot on the P-P volume indicates a complex channel system. The Vp/Vs value from automatic analysis around this horizon also gives indications of the channel sands as a low value (Figure 12).
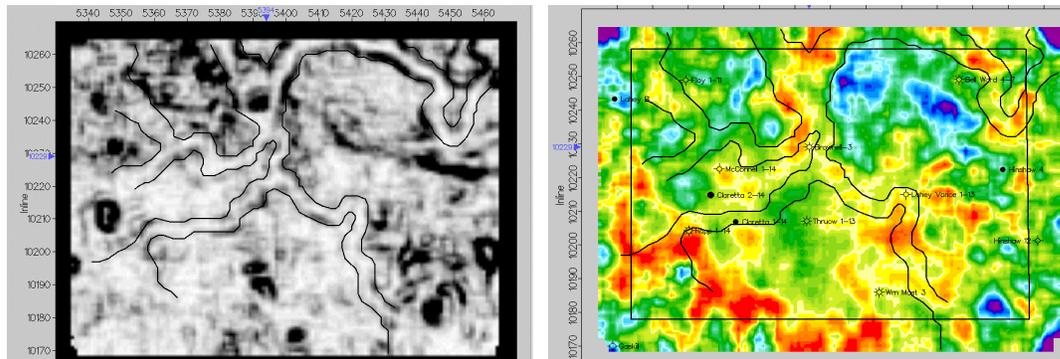
Figure 12. Maps of the St. Gen horizon. A coherency plot derived from the P-wave data (left) indicating a channel system with the corresponding Vp/Vs plot (right) automatically calculated over a 100 ms window. The red and yellow values indicate a low Vp/Vs value.

Fluids

Thompson et al. (2000) present early results from a 30 km 2-D multicomponent line, in 750 m of water, shot over the Fles Dome, offshore Norway. There is a flat

spot in the P-P data set that is an area of continuous stratigraphy on the P-S section. This suggests a DHI of a fluid contact (Figure 13).
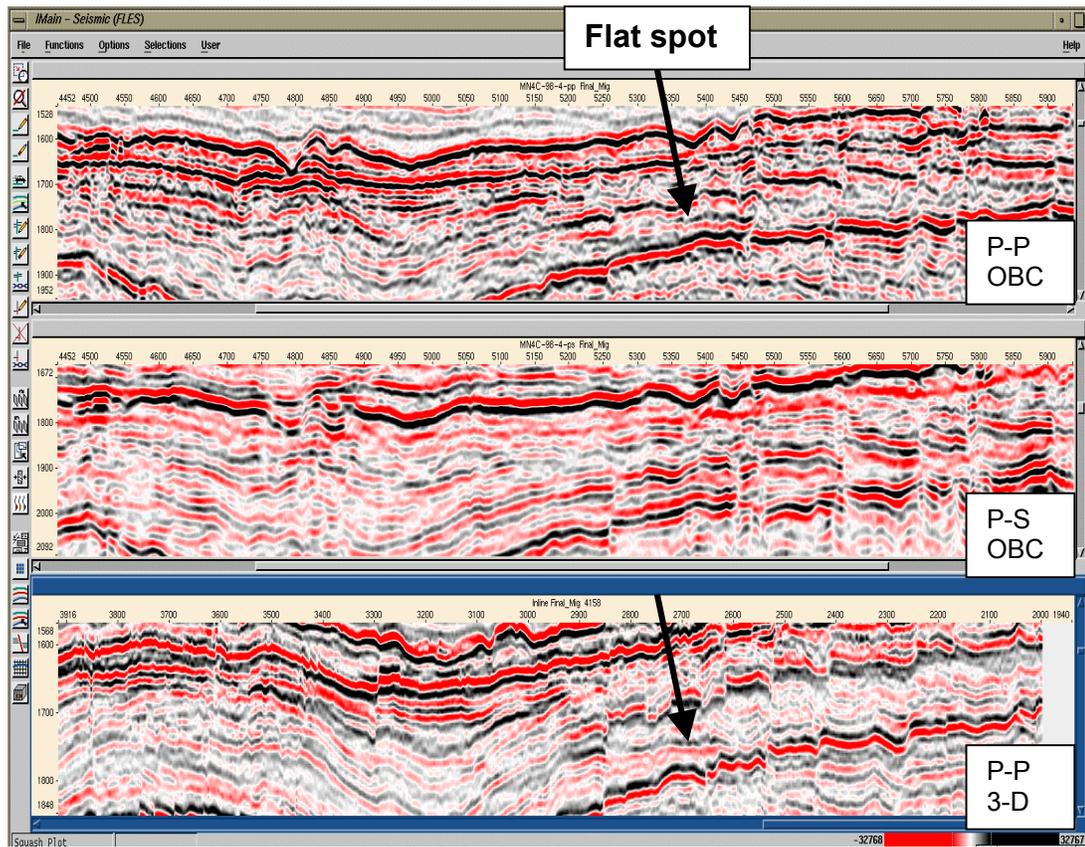
Figure 13. Flat spot analysis on P-P and P-S from the Fles prospect, offshore Norway (Thompson et al., 2000). The top section is the P-wave data from the 2-D OBC survey, the middle section is the P-S data from the OBC survey, and the bottom section is a line extracted from a 3-D towed streamer volume.

Todorov and Stewart (2000) use the Blackfoot 3C-3D seismic data to estimate oil column height. They first pick a P-P isochron in a region (Mannville to Mississippian) surrounding the reservoir. This isochron provides a regular and dense data set complementary to the sparse isopach values from the well logs over the same Mannville-Mississippian interval. The isochron is then co-kriged with isopach values from well logs. The isochron is thus converted to a regularly sampled and dense isopach. The Vp/Vs value is next computed using isochron ratios from the P-P and P-S data over the same area. This Vp/Vs value is, in turn, co-kriged with the gamma ray index to give an areal estimate of the shale content. Note that the gamma ray index is converted to a shale content using sand and shale lines and linear interpolation of values between them. The clastic interval (the isopach under consideration) is assumed to consist only of shale and sand. Thus, the sand estimate is one minue the shale percentage. Amplitude inversions are conducted on both P-P and P-S volumes to determine P- and S-wave velocities, respectively. The P-P, P-S, Vp inversion, and Vs inversion volumes plus porosity logs are then used to predict porosity values over the interval using a neural net. The average water saturation (Sw) in the reservoir,

which is 25%, is used to infer the oil saturation (1 - %Sw). Finally, the oil column height (OCH) for every seismic point estimated using the product of these factors: OCH = isopach x %sand x porosity x oil saturation as shown in Figure 14. Note that using a 3.0 m cut-off value, they estimated the volume of oil in place at about 1.2 x 10^6 m^3. The engineering report using the original 3-D seismic and about one year of production data estimated a value of 1.36 x 10^6 m^3.
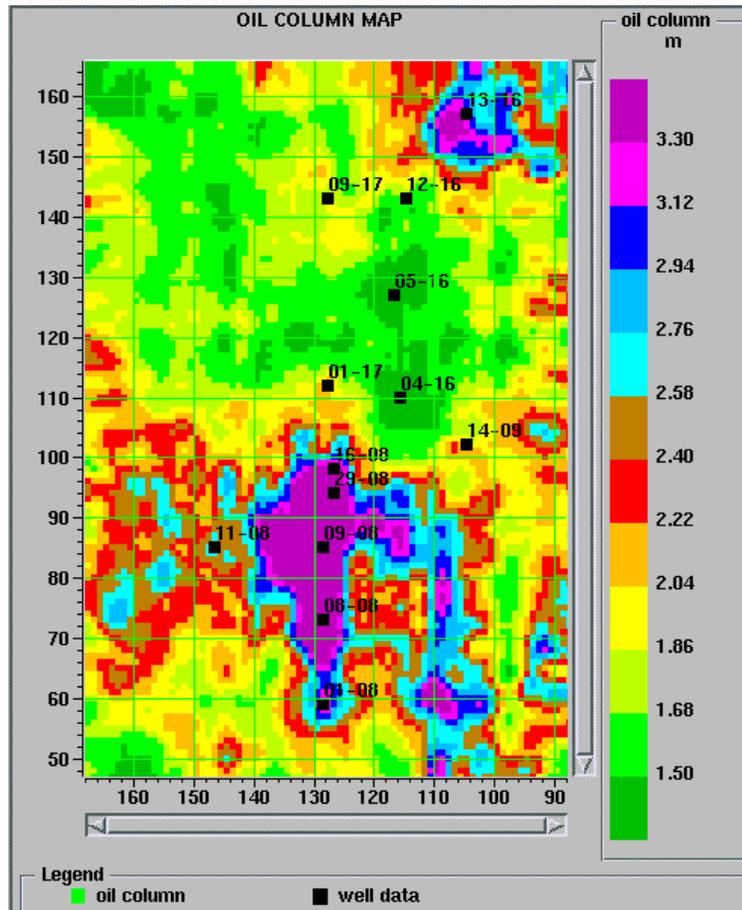
Figure 14. Oil column height (OCH) estimation determined from OCH = isopach x %sand x porosity x oil saturation.

Poor *P*-wave areas (gas-charged sediments)

P-wave energy can be scattered and attenuated when passing through gas-saturated strata. Whether in the near-surface or just above the reservoir, gas-saturated sediments can seriously degrade imaging of deeper features.

Some areas in the North Sea have near-surface channels apparently containing biogenic gas that saturates poorly consolidated sediments (Figure 15). Although these hydrocarbon deposits are not economic, they are of interest because of their deleterious effect on conventional *P*-wave images. Reflections from interfaces within and below the gas-charged channels are extremely poor on the stacked *P*-wave

section, exhibiting reverberations and attenuation of high frequencies. In contrast, the *P-S* section delineates the channel base, interfaces below the channel, and even sediment boundaries within the channel.
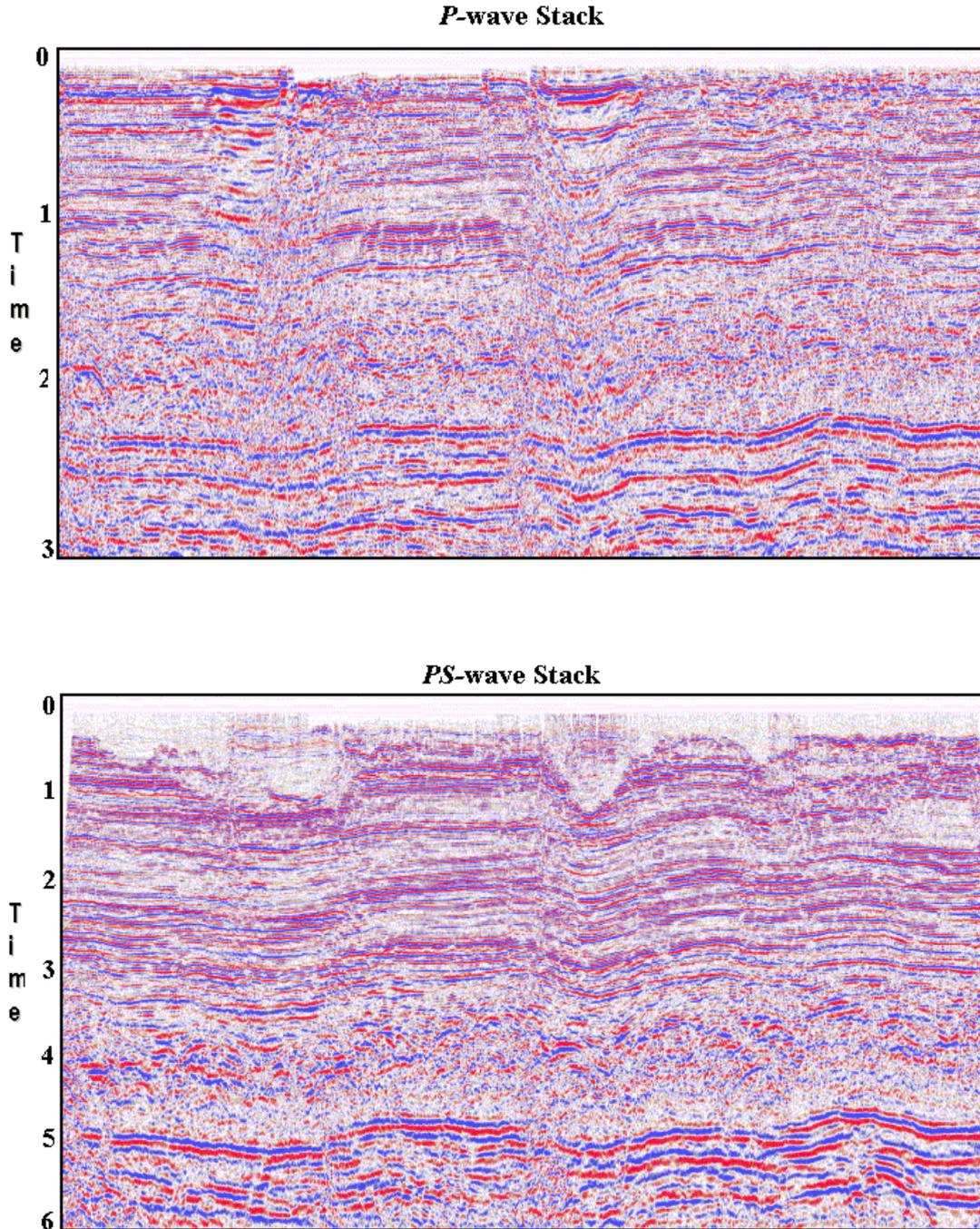
Figure 15. Comparison between *P*-wave and *P-S* 2-D section over North Sea shallow-gas channels. *P*-waves exhibit reverberations and high frequency attenuation, but *P-S* section delineate the channel base, interfaces below the channel, and even sediment boundaries within the channel.

Leaky gas reservoirs can release a gas plume which makes conventional imaging and characterization of the reservoir very difficult. *S*-waves, on the other hand, are generally less sensitive to rock saturants and can be used to penetrate gas-saturated sediments as shown previously. The SUMIC (sub-sea seismic) technique used 3-C geophones planted on the ocean bottom (Berg et al., 1994). From these recordings, *P-S* images were constructed. Remarkable examples of this imaging through a gas chimney (Granli et al., 1995) have led to an enormous interest in marine shooting with ocean-bottom cables (OBC) and sub-sea seismometers.
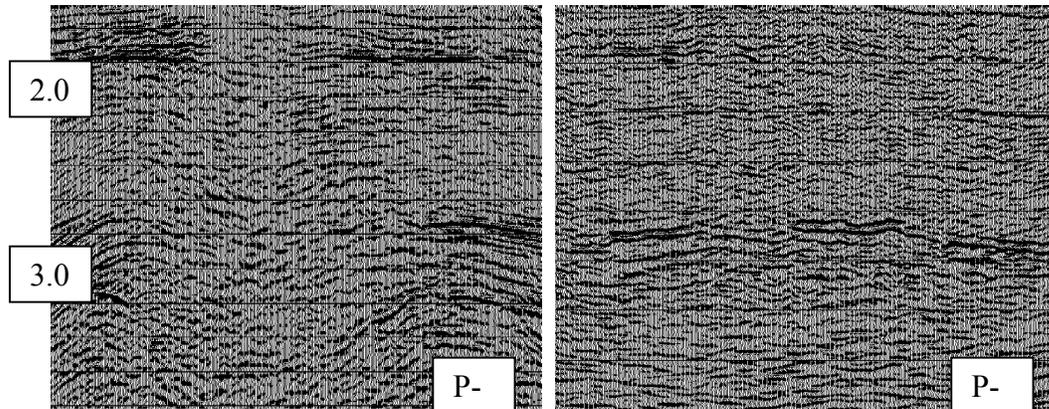
Figure 16. P-P and P-S sections from the Valhall field, Norway showing improved imaging across the anticlinal structure (after Rodrigues, 2000).

Rodriguez Saurez (2000) shows a case from the Valhall field, Norway. He used equivalent-offset migration (EOM) for converted waves to image through a case cloud. The results provide a more interpretable image through the gas cloud and anticlinal reservoir top at about 2.8 s on the P-wave section (Figure 16).

In cases where there are high-velocity layers – volcanics (e.g., basalts), carbonates, salts, or even permafrost in the near surface, seismic imaging may be complicated or compromised. Purnell (1992) uses a physical model with a single high-velocity layer to demonstrate some of the modes that are observed in such a case. *P*-waves convert to *S*-waves with high efficiency going from low- to high-velocity layers. He finds that when migration is targeted to use these events (*SPPS*, *SPPP*, *PPPS*) some significantly improved images can be obtained.

Structural imaging

Resolution of steeply dipping features can be improved using converted waves in certain circumstances. Purnell (1992) shows examples from physical modelling data where high angle anomalies were more visible on migrated *P-S* data than on migrated *P-P* data. High-velocity near surfaces also have the potential to allow both *P* and *S* energy to propagate at angles away from the vertical. This puts the *P-P* and *P-S* energy on both vertical and radial channels.

Cary and Couzens (2000) show examples from the Mahogany field in the Gulf of Mexico where *P-S* images show excellent definition of faults associated with salt intrusion (Figure 17). The *P*-wave section provides a more resolved image deeper in the section. Improving *P-S* images at depth is a research challenge.

(a)   (b)
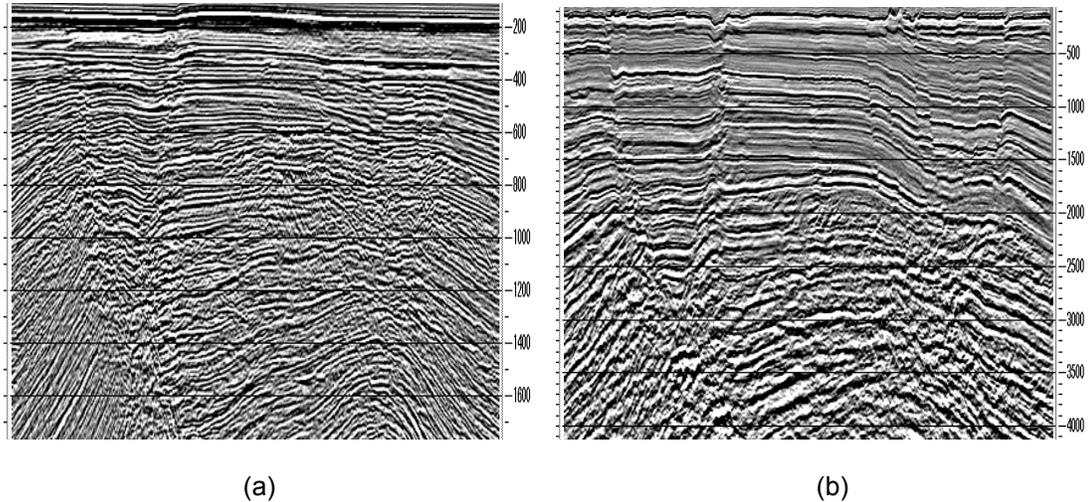
Figure 17. (a) Poststack migrated stack of geophones component from the Mahogany field. (b) Poststack time migration of depth-variant CCP stack of X-component from the Mahogany field (from Cary and Couzens, 2000).

Le Stunff et al. (2000) applied traveltime reflection tomography to build both P- and S-wave velocity models in depth. They then used these velocities to create pre-stack depth migration images from the East Natuna Basin in Indonesia. The P-S image shows a remarkable anticlinal structure (Figure 18). They also use common image gather in depth to check the validity of the velocity model.
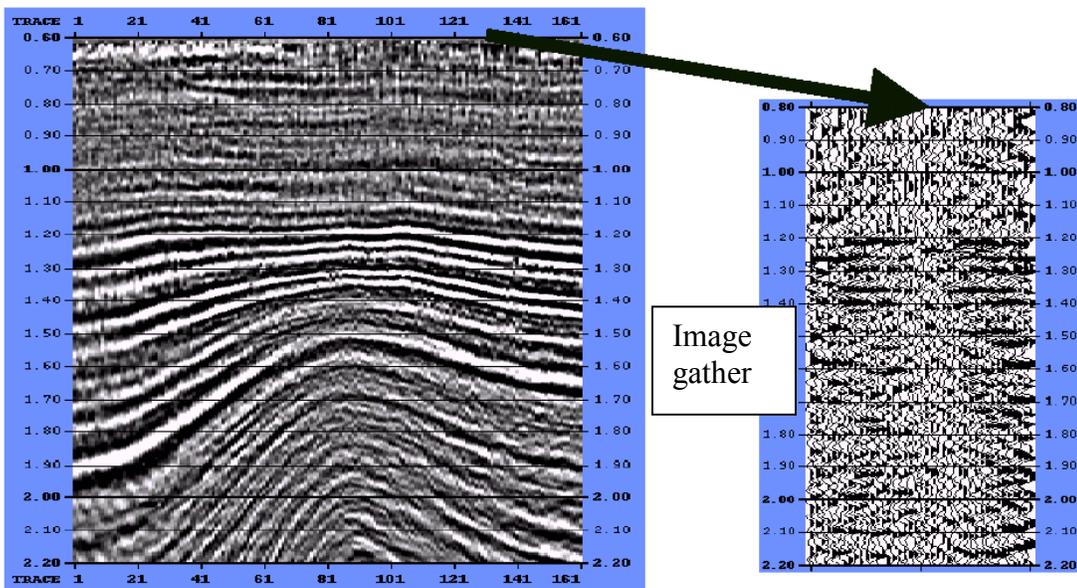
Figure 18. P-S image from the East Natuna Basin in Indonesia (Stumpf et al. 2000). An image gather (right) indicates well flattened events and thus an appropriate velocity field.

Jin and Michelena (2000) describe a prestack inversion technique that uses automatic velocity building, a ray_Born prestack depth migration, and AVO inversion from the common-angle migrated gathers. They test this approach on the Mahogany data set to image a salt body (Figure 19).
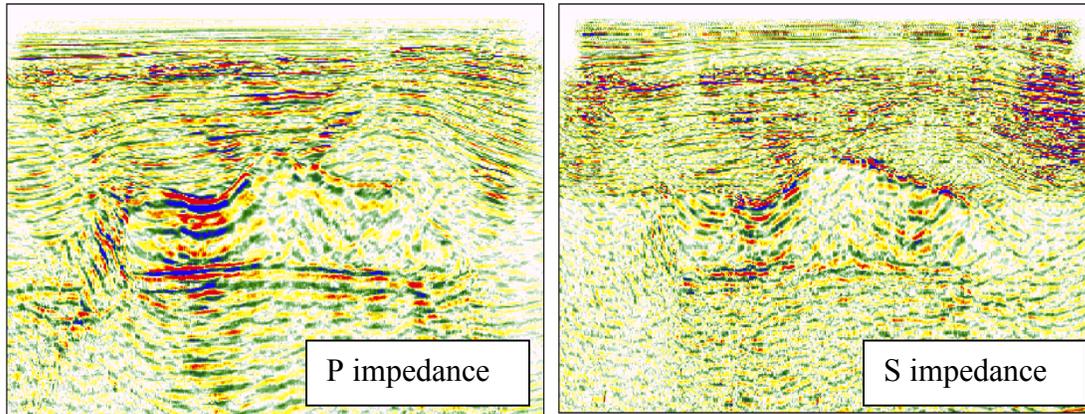
Figure 19. P-P and P-S migration and inversion results from the Mahogany 4C-2D survey in the Gulf of Mexico (Sin and Michelena, 2000). The P-wave impedance, from the P-wave data, on the left and S-wave impedance derived from P-S data (right) show the general outline of an encased salt body.

Anisotropy and fracture analysis

Gaiser (2000) shows the results of applying Alford rotation and layer stripping (where off-diagonal components are minimized) to data from the Teal South, Gulf of Mexico 4C-4D survey. A receiver gather in Figure 20 indicates the amount and direction of the anisotropy.
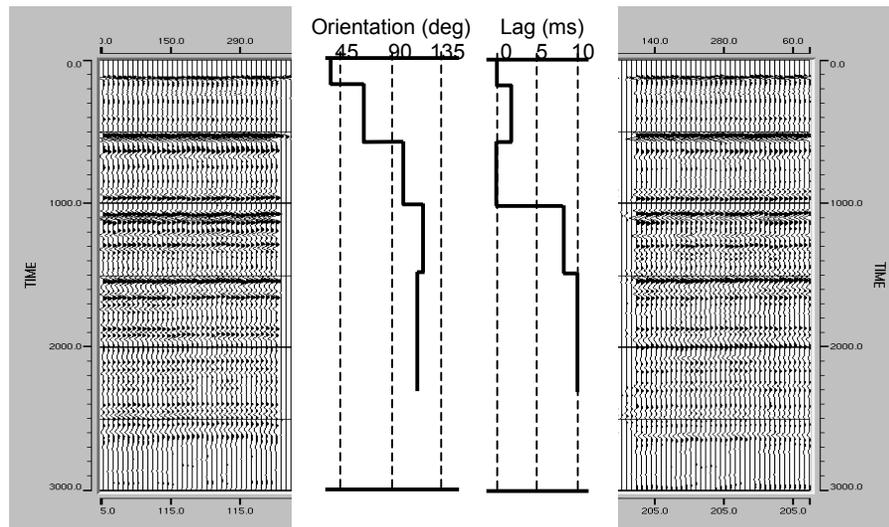
Figure 20. Anisotropic rotations on a receiver gather from the Teal South survey. The slow S-wave (P-S$_2$) on the right has been stretched to fit the fast converted wave on the left. The total amount of anisotropy and its direction is shown in the middle panel.

   Ata and Michelena (1995) show an example of three 3-C seismic lines arranged in a star pattern in Venezuela. After processing and analysing the data, they find indications of fracture direction from their calculated anisotropy.

   Gaiser (1999) and Van Dok et al. (1997) show analyses of a full 3C-3D seismic survey from the Madden field in the Wind River Basin, Wyoming. This analyses uses 4-component Alford (1986) rotations and layer stripping (Winsterstein and Meadows, 1991a) to calculate the fast shear-wave (P-S_1) polarization direction and the associated percent anisotropy. Figure 21 is a portion of the data from an east-west line: the radial and transverse polarization for east-west propagation. There are equivalent sections for north-south propagation. To compensate for the effects of depth varying properties (Winterstein and Meadows, 1999b), the reflection at 1.5 seconds is analyzed first to remove shear-wave splitting effects from the overburden. Although the energy on the transverse component for this event is weak in places, removing overburden effects from the target reflections below is an important step to unravel shear-wave birefringence. Figure 22 shows the fast S-wave direction and its associated percent anisotropy, corresponding to possible fracture orientation and fracture density of the target horizons between 2.2 and 3.3 seconds. Regions of high percent anisotropy (9% or more) correlate well with the known east-west trending faults superimposed on the maps.
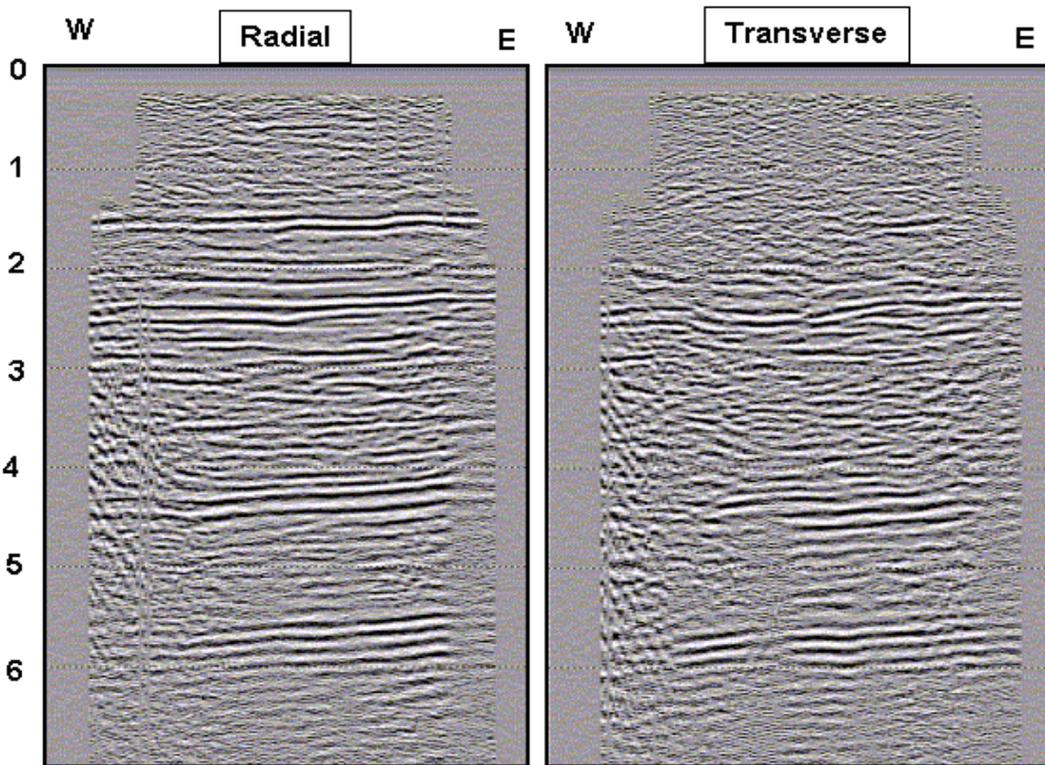
Figure 21. Radial and transverse receiver components for east-west propagation from a 3-D survey at the Madden field in Wyoming. Using equivalent sections for north-south propagation.
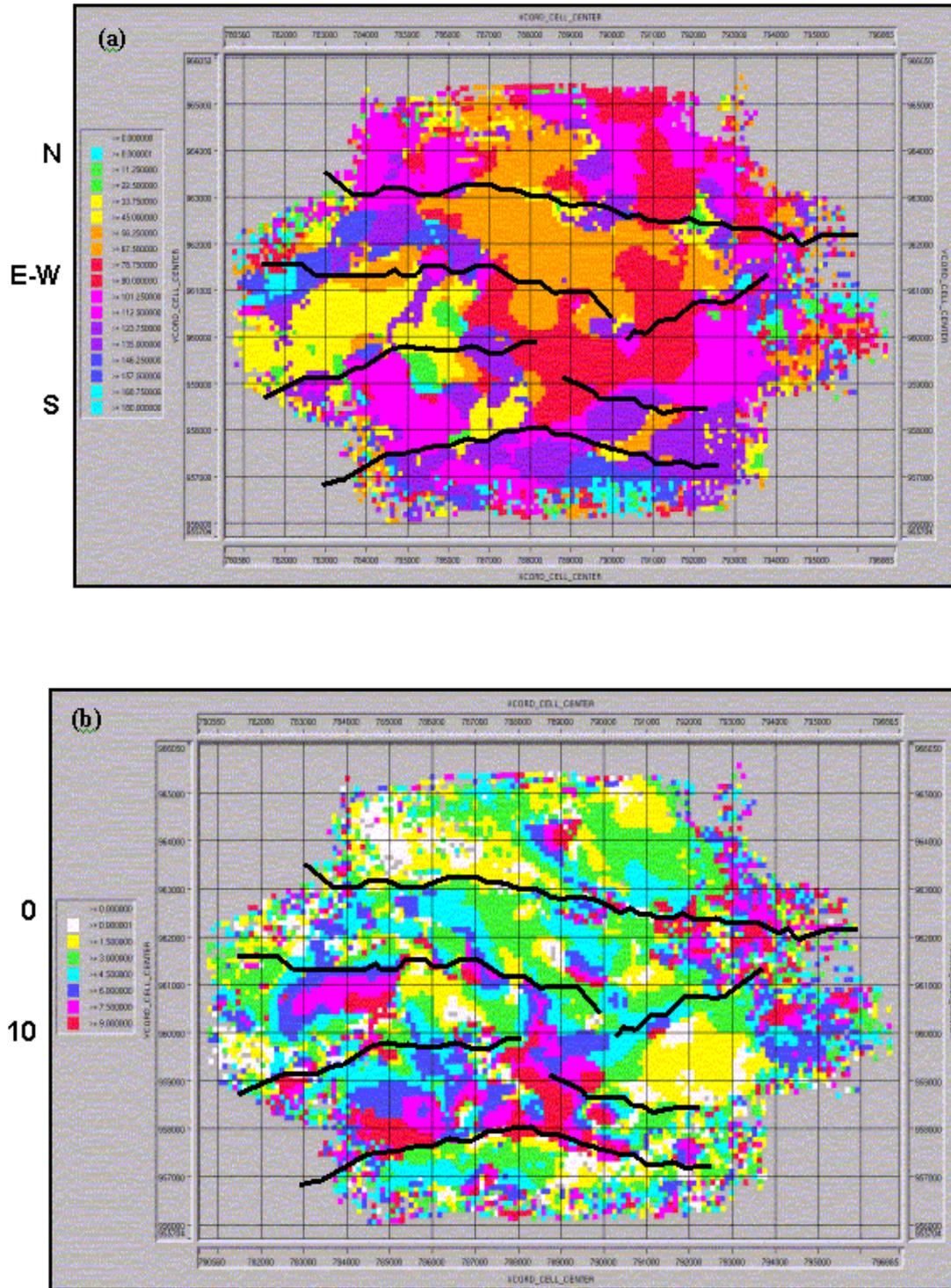
Figure 22. Seismic anisotropy calculated by Alford rotation and layer stripping from the data in Figure 21, after removing the birefringence effects of the overburden. Fast *S*-wave (*P*-*S₁*) polarization direction (a) and percent azimuthal anisotropy (b) for the target layer between 2.2 and 3.3 seconds. Regions of high percent anisotropy (9% or more) correlate well with the known east-west trending faults superimposed on the maps.

As in many situations, there is an issue of resolution. These fracture property estimates are an average over 1.1 seconds of data – an interval clearly larger than the reservoirs of interest. Fracture detection at finer intervals can be attempted by careful survey design, providing optimal fold, offset and azimuthal distribution.

Numerical modelling (Li et al., 1996) suggests that gas-saturated oriented fractures may have a distinct effect on *P-S* velocity (Figure 23). This is in contrast to conventional isotropic thinking, where fluid saturation has little impact on *S*-wave velocities. Guest et al. (1998) interpret anomalies in *S*-wave splitting over a gas reservoir in Oman as evidence of an effect of gas on shear waves.

Probert et al. (2000) show anisotropy indicated in a North Sea 4C-3D seismic project.
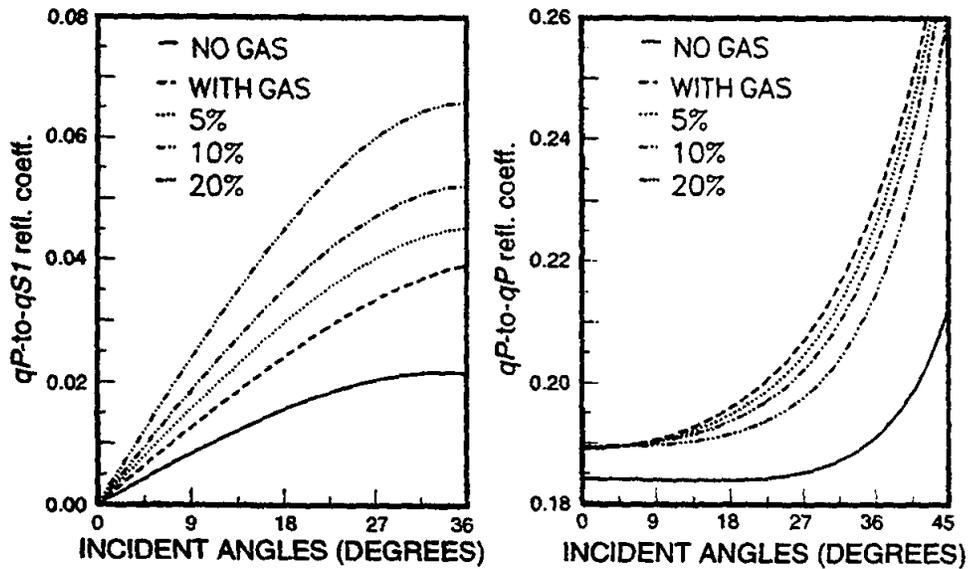
Figure 23. Theoretical modeling for gas-saturated fractured material indicating that anisotropy may have a large effect.

Reservoir monitoring

Isaac (1996) shows *P-P* and *P-S* sections from a heavy-oil reservoir at Cold Lake, Alberta that is undergoing steam flooding (Figure 24). There are variations in the reservoir rock properties associated with temperature and saturation changes. These, in turn, are associated with changes in the seismic character of both *P-P* and *P-S* sections. Using repeated surveys, she found that V_p/V_s could discriminate between hot, warm, and cold parts of the reservoir (Figure 25).
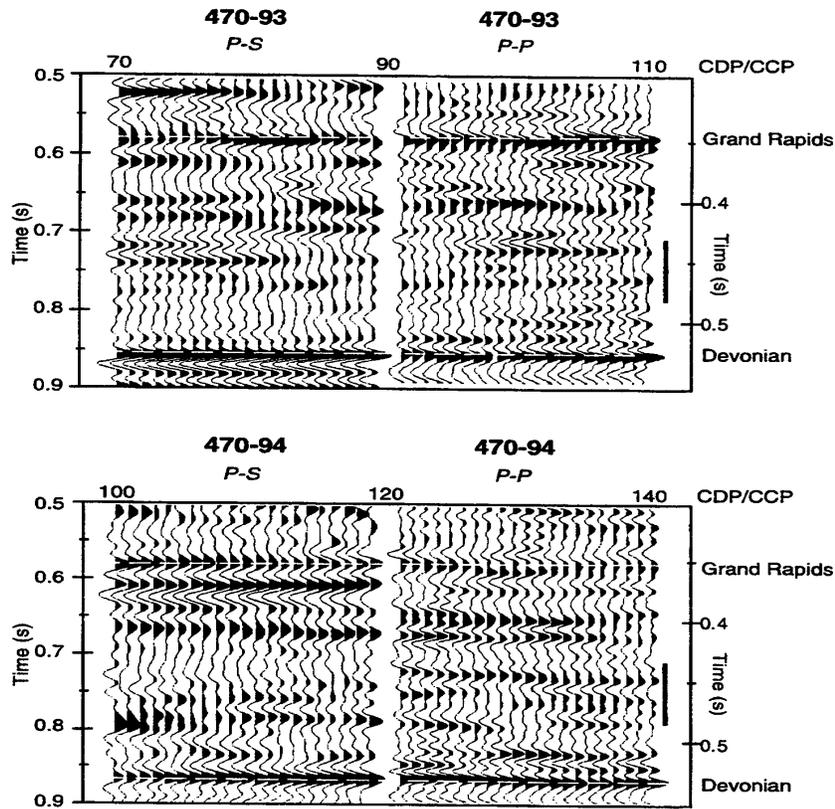
Figure 24. Comparison of the 1993 and 1994 seismic lines. Note the similar data quality and resolution among all lines (from Isaac, 1996).
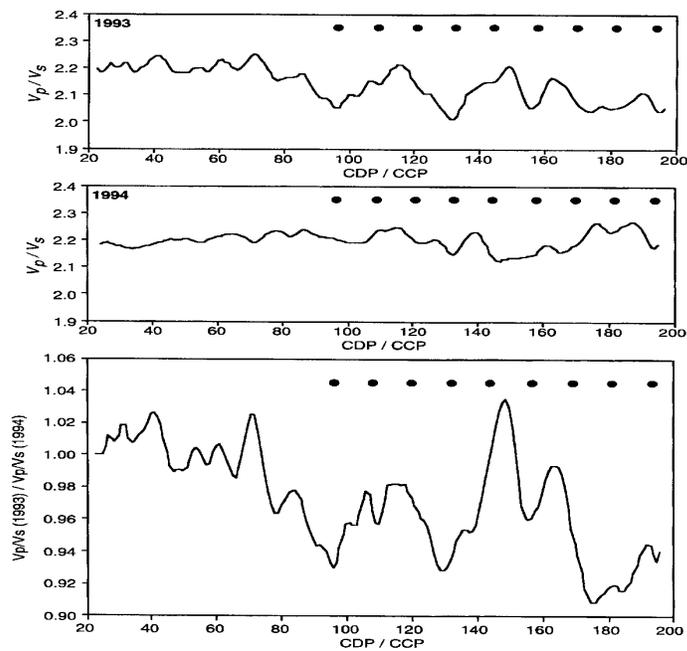
Figure 25. V_p/V_s plots for 1993 lines, 1994 lines, and the ratio of those two. Note that the V_p/V_s value is generally lower in the unsteamed regions away from the wells (from Isaac, 1996).

Spitz et al. (2000) discuss results from a 4C-4D survey conducted over the Teal South field, Gulf of Mexico. There were two 4C-3D surveys, in 1997 and 1999, conducted by the Energy Research Clearing House (ERCH) in Houston. This pioneering study shows time-lapse differences in the fast converted wave (P-S_1) component of the Teal South 4C-4D seismic (Figure 26).
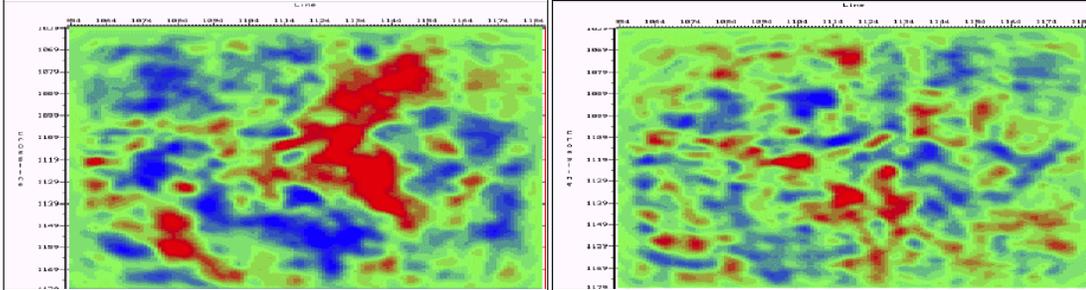
Figure 26. Fast, converted-wave (P-S_1) time slices from the Teal South, Gulf of Mexico 4C-4D survey at the reservoir level. The P-S image from 1997 (left) is subtracted from the 1999 image to give the difference on the right.

WHAT'S LEFT TO DO

Converted-wave exploration has come a long way in the last several years. But, there's still a lot of room left for progress. Further applications await surveys and sections in novel environments or analysis of existing images for other targets. In addition, there are many other modes that propagate in a seismic survey – such as an S-wave leg through a high-velocity region. We can make pictures (Figure 27) from
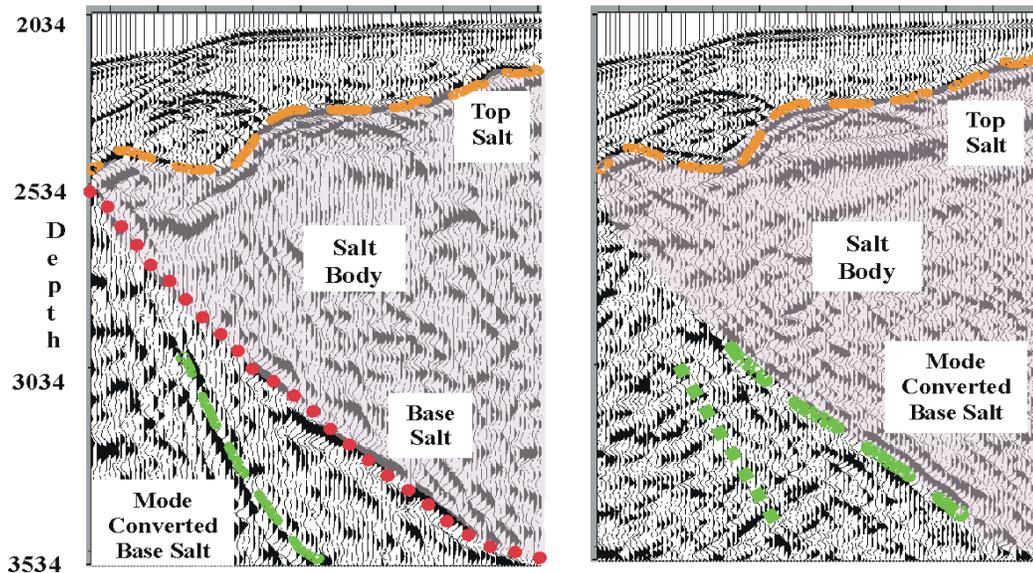
Fig. 27. Comparison of prestack depth-migrated streamer data using *P*-wave and *S*-wave salt-velocity models. Migration with an *S*-wave velocity model images *PSSP* waves that have converted at the top of the salt. The position of the *S*-wave event at the base of the salt is in agreement with the *P*-wave image.

this more complicated conversion as in the Gulf of Mexico, where a P-wave converting to an S-wave inside a salt volume has been used to create an image.

CONCLUSIONS

The reflection seismic method has used *P*-waves for many years – and with great success. However, there is more to be done in exploration seismology, especially by using the other elastic modes that are part of the seismic survey (particularly the *P-S* waves). *P-S* seismic exploration is showing many new examples of successful cases of imaging and hydrocarbon-related interpretation. Particularly well documented cases exist for sand/shale discrimination, gas-cloud imaging, and anisotropy analysis.

ACKNOWLEDGMENTS

REFERENCES

Alford, R.M., 1986, Shear data in the presence of azimuthal anisotropy: Dilly, Texas, 56th Ann. Internat. Mtg., Soc. Expl. Geophys., Houston, S9.6, 476-479.

Ata, E. and Michelena, R.J., 1995, Mapping distribution of fractures in a reservoir with *P-S* converted waves: The Leading Edge, **14**, 664-676.

Berg, E., Svenning, B., and Martin, J., 1994, SUMIC: Multicomponent sea-bottom seismic surveying in the North Sea – Data interpretation and applications: Presented at the 64th Ann. Intl. Mtg., Soc. Expl. Geophys., Expanded Abstracts, 477-480.

Cary, P.W. and Couzens, R.A., 2000, Processing 4-C data from Mahogany Field, Gulf of Mexico: Presented at the SEG/EAGE Summer Research Workshop, Boise, Idaho.

Frasier, C. and Winterstein, D., 1990, Analysis of conventional and converted mode reflections at Putah Sink, California using three-component data: Geophysics, **55**, 646-659.

Fyfe, D.J., Dent, B.E., Kelamis, P.B., Al-Mashouq, K.H., and Nietupski, D.A., 1993, Three-component seismic experiments in Saudi Arabia: Presented at the 55th Ann. Mtg. Europ. Assn. Expl. Geophys.

Gaiser, J.E., 1999, Applications for vector coordinate systems of converted waves obtained by multicomponent 3-D data, 31st Ann. Off. Tech. Conf., Houston, OTC 10985.

Gaiser, J.E., 2000, Advantages of 3-D PS-wave data to unravel S-wave birefringence for fracture detection: Presented at the SEG/EAGE Summer Research Workshop, Boise, Idaho.

Garotta, R., Marechal, P., and Magesan, M., 1985, Two-component acquisition as a routine procedure for recording *P*-waves and converted waves: Can. J. Expl. Geophys., **21**, 40-53.

Goodway, W. and Tessman, D.J., 2000, Blackfoot 3C/3D, a VectorSeis case history: Presented at the SEG/EAGE Summer Research Workshop, Boise, Idaho.

Granli, J.R., Sollid, A., Hilde, E., and Arnsten, B., 1995, Imaging through gas-filled sediments with marine *S*-wave data: Expanded Abst., 65th Ann. Intl. Mtg., Soc. Explor. Geophys.

Guest, S., Vander Kolk. C., and Potters, H., 1998, The effect of fracture filling fluids on shear-wave propagation: Presented at 68th Ann. Intl. SEG Mtg., Expd. Abst., 948-951.

Isaac, J.,H, 1996, Seismic methods for heavy oil reservoir monitoring: Ph.D. thesis, The Univ. of Calgary.

Jin, S. and Michelena, R.J., 2000, Prestack inversion of multicomponent data from complex structure: Mahogany Field example, Gulf of Mexico: Presented at the SEG/EAGE Summer Research Workshop, Boise, Idaho.

Kendall, R.R., Gray, S.H., and Murphy, G.E., 1998, Subsalt imaging using prestack depth migration of converted waves: Mahogany Field, Gulf of Mexico: Presented at 68th Ann. Intl. SEG Mtg., Expd. Abst., 2052-2055.

Kristiansen, P., 2000, 4 years experience with 4C seismic: what we have learned: Presented at the SEG/EAGE Summer Research Workshop, Boise, Idaho.

Le Stunff, Y., Gosselet, A., Nguyen, S., Berthet, S., and Boelle, J.L., 2000, 3D PP and PS travel time reflection tomography on a case study: Presented at the SEG/EAGE Summer Research Workshop, Boise, Idaho.

Li, X., Kuhnel, T., and MacBeth, C., 1996, Converted-wave AVO and its implications: Extd. Abst., 58th Ann. Intl. Mtg., Europ. Assn. Geosci. Eng., M046.

MacLeod, M.K., Hadley, M.J., Reynolds, K.J., and Tura, A., 1999a, Multicomponent analysis of OBC data, 31st Ann. Off. Tech. Conf., Houston, OTC 10940.

MacLeod, M.K., Hanson, R.A., Bell, C.R., and McHugo, S., 1999b, The Alba field ocean bottom cable seismic survey: Impact on development, Off. Euro. Conf., Aberdeen, SPE 56977.

Miller, S.L.M., 1996, Multicomponent seismic data interpretation: M.Sc. thesis, University of Calgary.

Miller, S.L.M., Harrison, M.P., Szata, K.J., Stewart, R.R., and Lawton, D.C., 1998, Interpretation of a carbonate reservoir using *P-P* and *P-SV* seismic data: Submitted to Geophysics.

Moldoveanu, N., Rink, U., and Van Baaren, P., 1998, Multicomponent acquisition in transition zone environment: an experimental study: Presented at 68th Ann. Intl. SEG Mtg., Expd. Abst., 738-739.

Nazar, B.D. and Lawton, D.C., 1993, AVO analysis of a thin conglomerate deposit: J. Seis. Expl., **2**, 333-348.

Nieuwland, F., Marschall, R., Papaterpos, M., and Sharp, D., 1994, An example of the use of shear waves in seismic exploration: J. Seis. Explor., 3, 5-20.

Probert, T., Ronen, S., and Bryan, R., 2000, A case study of azimuthal anisotropy analysis from a N. Sea 3D 4C project: Presented at the SEG/EAGE Summer Research Workshop, Boise, Idaho.

Purnell, G.W., 1992, Imaging beneath a high-velocity layer using converted waves: Geophysics, **57**, 1444-1452.

Rodriguez Saurez, C., 2000, Advanced marine methods: Ocean-bottom and vertical cable analyses: Ph. D. thesis, University of Calgary.

Spitz, S., Gratacos, B., Haggard, W., and Vuillermoz, C., 2000, Reservoir monitoring using multicompoinent seismic: Processing the Teal South 4D-4C: Presented at the SEG/EAGE Summer Research Workshop, Boise, Idaho.

Stewart, R.R., Ferguson, R., Miller, S.L.M., Gallant, E., Margrave, G., 1996, The Blackfoot seismic experiments: Broad-band, 3C-3D, and 3-D VSP surveys: CSEG Recorder, 6, 7-10.

Tatham, R.T., 1982, V_p/V_s and lithology: Geophysics, **47**, 336-344.

Thomsen, L., 1999, Converted-wave reflection seismology over inhomogeneous anisotropic media: Geophysics, **64**, 678-690.

Thompson, C., Helgesen, H.K., and Battie, J.E., 2000, 2D-4C seismic exploration data for risk reduction, Fles prospect, offshore Mid-Norway: Presented at the SEG/EAGE Summer Research Workshop, Boise, Idaho.

Van Dok, R.R., and Gaiser, J.E., 2000, Stratigraphic description of the Morrow formation using mode-converted shear waves: Interpretation tools and methods for three land surveys: Presented at the SEG/EAGE Summer Research Workshop, Boise, Idaho.

Van Dok, R.R., Gaiser, J.E., Jackson, A.R., and Lynn, H.B., 1997, 3-D converted-wave processing: Wind River Basin case history, 67th Ann. Internat. Mtg., Soc. Expl. Geophys., Dallas, SP5.4, 1206-1209.

Valenciano, A.A., Banchs, R.E., and Michelena, R.J., 2000, Facies recognition using PP and PS stratigraphic inversion: Presented at the SEG/EAGE Summer Research Workshop, Boise, Idaho.

Winterstein, D.F. and Meadows, M.A., 1991a, Shear-wave polarizations and subsurface stress directions at Lost Hills field, Geophysics, **56**, 1331-1348.

Winterstein, D.F. and Meadows, M.A., 1991b, Changes in shear-wave polarization azimuth with depth in Cymric and Railroad Gap oil fields, Geophysics, **56**, 1349-1364.